A.B. Nadtochiy[1], B.M. Gorelov[2], O.I. Polovina[1], S.V. Shulga[2], O.O. Korotchenkov[1], A.M. Gorb[1]

Sound Velocities in Graphene-Based Epoxy Nanocomposites

[1]Taras Shevchenko National University of Kyiv, Kyiv, Ukraine, nadtku@univ.kiev.ua
[2]Chuiko Institute of Surface Chemistry, NAS of Ukraine, Kyiv, Ukraine, bgorel@ukr.net

Elastic properties of epoxy-based nanocomposites (ENCs) filled with bare and TiO_2-deposied multi-layered graphene nanoplatelets (MLG) have been tested by using a phase-frequency continuous-wave ultrasound probing (USP). The dian epoxy CHS-EPOXY 520 curried with diethylenetriamine (DETA) was the polymer matrix for the nanocomposites. The nanoplatelets of the specific surface area $S_f \sim 790$ m^2/g consist of several dozen loosely bound monoatomic graphene layers with an area of about least 5×5 μm^2. MLG-mass-loading ($\varphi_{f,m}$) of the nanocomposites varied from 0.1 % to 5.0 % by weight. Anatase- TiO_2 particles, being of about 50 nm in diameter and of $S_f \sim 1500$ m^2/g, have been deposited on MLG in mass concentration of about 1 %.

Elastic moduli of the ENCs (namely, the Lame's constants, the Young's module, the compression module, and the Poisson's ratio) have demonstrated negligible variation with $\varphi_{f,m}$ varying regardless the type of filling particles. However, MLG:TiO_2-hybrid nanoparticles have proven to impact stronger on the moduli as compared to bare MLG. This result shows a capability to modify molecular structure of epoxy resins by controlling surface reactivity of MLG embedded in the resin.

Keywords: multi-layered graphene nanoplatelets, anatase nanoparticles, epoxy-based nanocomposites resin, ultrasound probing, elastic moduli.

Introduction

The polymer nanocomposites (PNCs) filled with either graphene particles or its derivatives (such as multi-layered graphene, graphene-oxide, or oxide-grafted graphene) still attract considerable interest due to possibility to tailor physical and chemical properties of PNCs encountered with only a small quantity of nanofiller incorporated to the host polymer matrix. From the other hand, the unique mechanical, thermal, and charge-transport properties of graphene in addition to an extremely high surface area and gas impermeability make the graphene as promising nano-sized filler for modifying molecular structure of polymers and, hence, for improving its mechanical, electrical, thermal, and gas barrier properties [1–11].

Graphene is a single-atom-thick sheet of sp^2–hybridized carbon atoms tightly packed in a two-dimensional (2D) honeycomb lattice with a carbon-carbon distance of 0.142 nm [12]. It has a high theoretical surface area of about 2630 m^2/g [13]. Recent experimental estimates obtained through nanoindentation measurements of free-standing monolayer graphene have indeed confirmed the predicted extreme elastic properties, namely 2D Young modulus $E_{2D} = 340 \pm 50$ N/m and the 2D breaking strength $\sigma_{2D} = 42 \pm 4$ N/m, leading to effective 3D values $E_{eff} = 1.0 \pm 0.1$ TPa and $\sigma_{eff} = 130 \pm 20$ GPa (considering the thickness of graphene as 0.335 nm), respectively [14]. Also, graphene has shown remarkable magnetic, electrical, and thermal properties [15].

In addition to above-mentioned unique properties, the recent developments on graphene synthesis routes and on the understanding of their unique properties have prompted the development and study of graphene filled nanocomposites. Therefore it is suggested that tailor-made functional and structural graphene-based nanocomposites which exploit the superlative properties of both graphene

filler and polymer host can show enhanced performance in a large number of applications ranging from flexible packaging, semi-conductive sheets in transistors, sensors, super capacitors, memory devices, hydrogen storage systems, printable electronics, etc. [3, 7, 16].

Numerous studies have shown that polymer nanocomposites filled with single layer graphene nanosheets (SLG), multi-layered or platelet graphene (MLG), as well as their oxides and chemically-modified derivatives exhibit substantial property enhancements at much lower loadings than with other conventional nano-fillers. In particular, MLG, which are stack of multiple graphene layers, is often used for reinforcement of polymers [17, 18] and for improving thermal conductivity of epoxy resins [19 −22]. As compared with SLG, MLG are available on the market at a significantly lower price and can play an important role in the industrial-scale applications [23]. Other advantages of MLG are the ability to tailor physical parameters by varying concentration, the morphological characteristics (such as aspect ratio, spatial orientation, number of layers), and chemical modification of the surface.

From the other hand, it is recognized in the literature, that the overall physical and chemical behavior of PNCs is significantly influenced not only by intrinsic properties, geometry, and spacial distribution of embedded nanoparticles, but also by the presence of so-called interphase layers (IPLs) arising in the vicinity of nanoparticles [24−27]. In particular, IPLs play an important role in governing the stress transfer over polymer-nanofiller interface and, thus, in controlling the failure mechanisms and fracture toughness of a PNC [2, 28].

Resuming our literature survey, it should be noted, that great number of above-mentioned factors influencing on overall properties of graphenic nanocomposites, and their interference, as well as a variety of polymer matrices used by various researches originate ambiguity in experimental results and hampers understanding of graphene-epoxy interfacial interaction mechanisms. It'clear that much experimental work should be done in order to reach better awareness on mechanisms underlying polymer network alteration in MLG-based PNCs. As a consequence, the peculiarities of MLG-epoxy interfacial interactions on a molecular level are still not thoroughly understood, leaving limited guidance on designing nanocomposites with intrinsically high functional performance and tailoring their operational characteristics for certain customer's needs.

Therefore, this study has been undertaken in order to obtain better awareness of MLG-epoxy interfacial interaction on molecular level from comparing loading effects of bare and TiO_2-deposited MLG-NPs on elastic modules of DGEBA-epoxy resin.

I. Experiment

1.1. Materials
MLG for our experiments have been prepared from the flakes of thermally expanded graphite by using the electrochemical technique described by Xia *et al.* [29]. To prevent the resulting MLG-material from oxidation it has

been kept as the suspension. The particles were about 5×5 μm in-plane dimensions, 50 nm in thickness, and of 790 m^2/g in specific surface area. The X-ray diffraction analysis showed that the MLG contain graphene sheets of about 40 single-atom thickness. The additional information can be found elsewhere [10] where preparation technique and morphological studies of MLG have been presented in details.

The TiO_2-anatase nanoparticles of 50-nm diameter have been deposited on MLG by adding the former into initial ethanol-based suspension of MLG before its ultrasonic treatment. The specific surface area of anatase particles was ~ 1500 m^2/g.

The commercially available CHS-EPOXY 520 (SpolChemie, a.s. Czech Republic) DGEBA-epoxy resin, of epoxy group content (E-Index) 5.21−5.50 mol/kg, EEW (Epoxy Equivalent Weight) 182−192 g/mol was used as the neat resin. Diethylenetriamine (abbreviated as Dien or DETA) has been used as a curing agent. DETA and is a nitrogen-containing organic compound with the formula $HN(CH_2CH_2NH_2)_2$ [30]. The epoxide to the hardener mass-ratio was kept to be constant at 7:1. Details of the curing process can be found elsewhere [31].

The MLG-mass-loading ($\varphi_{f,m1}$) for both nanocomposite sets was 0.5 %, 1 %, 2 %, and 5 %, whereas the TiO_2-mass loading ($\varphi_{f,m2}$) varied as 0.5 %, 1 %, and 5 %. As-prepared liquid composites of both the types were ultrasonically mixed until homogeneous suspensions were obtained, then were vacuumated in order to remove ethanol and treated by ultrasound again. After adding the hardener into the mixture, the further polymerization of the mixture occurred at a room temperature during 72 hours. Cylindrically-shaped nanocomposite's samples of about 7 mm in diameter and 10-20 mm in length have been used for ultrasound studies. The samples were shortened to the required length and polished after polymerization.

1.2.   The measuring technique
Acoustic parameters of samples under study have experimentally been investigated by measuring phase velocities (V) of various types of elastic waves at room temperatures.

V–measurements for longitudinal (V_L) and shear (V_S) waves were performed by the phase-frequency technique in a continuous wave mode of operation [32]. The experimental set-up is shown on Fig. 1.
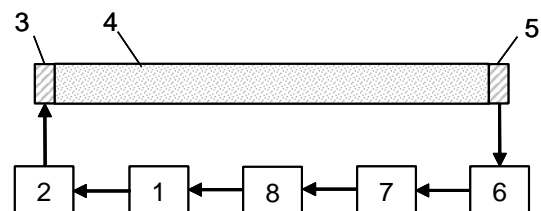
Fig. 1. Experimental set-up for exciting and measuring bulk waves in a continuous wave mode of operation.

The experimental set-up contains a PC-controlled frequency synthesizer AD9850 (1) which feeds the input piezoelectric transducer (3) via a power amplifier (2). An

excited elastic wave of the circular frequency $\omega=2\pi f$ propagates along the sample 4 and is then detected with the receiving piezoelectric transducer 5, 6 – the receiver. The frequency-dependent phase shift $\Phi(\omega)$ between input (U_{in}) and output (U_{out}) electric signals was detected with the phase detector (7), digitized, and transferred into a computer (8) for data-acquisition, processing, and computing frequency-dependent physical characteristics described below. The measurements have been carried out within the frequency range of 1.0 – 2.0 MHz where ultrasound vibrations suffer both negligible dispersion and high attenuation. Different pairs of transducers were used to excite longitudinal and shear waves separately.

For every case, frequency dependencies of the group delay time (T_g) and the group velocity (V_g) have been determined by using the well-known relations [33]:

$$T_g(\omega) = \frac{d\Phi(\omega)}{d\omega}, \qquad (1)$$

$$V_g(\omega) = \frac{d\omega}{dk} = \frac{L_S}{T_g(\omega)}, \qquad (2)$$

where $k(\omega)$ are the wave number.

$$k(\omega) = \frac{\Phi(\omega)}{L_S}, \qquad (3)$$

and L_S is the sample's thickness. Then, the correspondent phase velocity $V(\omega)$ can be evaluated from the relation [34]:

$$\frac{1}{V_g(\omega)} = \frac{1}{V(\omega)} - \frac{\omega}{V^2(\omega)} \frac{dV(\omega)}{d\omega}. \qquad (4)$$

In a case of negligible dispersion $dV(\omega)/d\omega \approx 0$ and (4) is reduced to $V(\omega) \approx V_g(\omega)$.

To exclude an overestimation of T_g due to wave propagation through both the transducers, both V_L– and V_S–measurement was made with two samples of different lengths (L_1 and $L_2= L_1/2$). By such the approach, the relation:

$$V_g(\omega) = \frac{L_1 - L_2}{T_{g1}(\omega) - T_{g2}(\omega)} \qquad (5)$$

has been used instead (4) to calculate $V_g(\omega)$. Here, both $T_{g1}(\omega)$ and $T_{g2}(\omega)$ were determined as inclination angle tangents of straight lines, which originated from the least-squares-approximated experimental $\Phi(\omega)$ – dependencies. The relative errors in T_g , V_L , and V_S did not exceed 1 %.

II. Results and Discussion

When the values of V_L and V_S have been measured, the Lame constants λ_C and μ_C have been evaluated via V_L and V_S and calculated value of composite's density ρ_C by using the formulae [33]:

$$\rho_C(\varphi_{f,v}) \cdot V_L^2(\varphi_{f,v}) = \lambda_C(\varphi_{f,v}) + 2\mu_C(\varphi_{f,v}) \quad (6a)$$

$$\rho_C(\varphi_{f,v}) \cdot V_S^2(\varphi_{f,v}) = \mu_C(\varphi_{f,v}) . \qquad (6b)$$

As maximal variations in ρ_C for both the MLG-filler (obtained for $\varphi_{f,v1}$=5.0 %) were no more than 0.4 %, we used calculated but not measured ρ_C –values. The values of $\rho_C(\varphi_{f,v})$ were calculated by using the formula which can be easily found from elementary considerations:

$$\rho_C = \rho_f\,\varphi_{f,v} + \rho_m(1 - \varphi_{f,v}), \qquad (7a)$$

Here, the volume-loading $\varphi_{f,v}$ have been calculated via the mass-loading by using well-known relation:

$$\varphi_{f,v1,2} = \frac{\varphi_{f,m1,2}}{\varphi_{f,m1,2} + \frac{\rho_{f1,2}}{\rho_m}(1 - \varphi_{f,m1,2})}. \qquad (7b)$$

Here, the subscripts "1" and "2" correspond to MLG-filled and MLG:TiO$_2$-filled, respectively.

In our calculations, $\rho_m = 1.2\cdot10^3$ kg/m^3 for epoxy [34], $\rho_{f1} = 2.267\cdot10^3$ kg/m^3 as a theoretical limit for graphene [35], and $\rho_{f2} = 4.2\cdot10^3$ kg/m^3 for TiO$_2$ [36].

Finally, a set of mechanical parameters including the Young's modulus E_C, the compression modulus K_C, and the Poisson's ratio v_C have been calculated via the Lame constants λ_C and μ_C by using the correspondent expressions which are valid for rod-shaped samples [37]:

$$v_C = \frac{1}{2(\lambda_C + \mu_C)}, \qquad (8a)$$

$$E_C = \mu_C \frac{3\lambda_C + 2\mu_C}{\lambda_C + \mu_C}, \qquad (8b)$$

$$K_C = \lambda_C + 2\mu_C/3 \qquad (8c)$$

From the physical point of view, knowledge about the Lame constants enables to evaluate the contribution from elastic strains d_{ij} into the free energy F of a material [38]:

$$F = \frac{\lambda_C}{2}\left(\sum_{i=1}^{3} d_{ii}\right)^2 + \mu_C \sum_{j=1}^{3}\sum_{k=1}^{3} d_{jk}^2. \qquad (9)$$

For applications, the Lame constants are widely used for predicting structural integrity of a material [39]. As to compressing module K_C and the Young's module E_C, the former characterizes an ability of material to vary its volume under all-round normal strain equalized in all direction (for example in a case of hydrostatic pressure), whereas the latter characterizes an ability of material to compress along an axis under the force applied along this axes [37]. Finally, the Poisson's ratio is a ratio of relative transversal compression to relative longitudinal tension of a rod-shaped sample under its mechanical loading along the rod's axis [37].

As can be seen from the Table 1a, noticeable variation in shear modulus and the Young's modulus take place at $\varphi_{f,v1} = 0.027$, whereas The Lame constant λ and the compression modulus K undergo negligible variations over the entire loading interval $0 < \varphi_{f,v1} \le 0.027$.

Increasing the elastic constants of the nanocomposites with increasing the loading evidences on alteration of their molecular structure due to particle-chain interactions at the interfaces. The most prominent alterations take place in a vicinity of the nanoparticles, where so-called interphase regions emerge. The interphase regions are being intensively studied by both experimental techniques

Measured phase velocities and calculated elastic moduli for MLG-epoxy nanocomposites.

$\varphi_{f,m1}$, [1]	$\varphi_{f,v1}$, [1]	V_S, $\times 10^{-3}$ m·s^{-1}	V_L, $\times 10^{-3}$ m·s^{-1}	μ_C, $\times 10^{-9}$ N·m^{-2}	λ_C, $\times 10^{-9}$ N·m^{-2}	v_C, [1]	K_C, $\times 10^{-9}$ N·m^{-2}	E_C, $\times 10^{-9}$ N·m^{-2}
0.000	0.000	1.19	2.68	1.70	5.22	0.303	6.35	3.76
0.005	0.0027	1.18	2.67	1.66	5.26	0.306	6.37	3.70
0.010	0.0053	1.19	2.69	1.71	5.35	0.305	6.48	3.79
0.020	0.0107	1.18	2.68	1.70	5.37	0.306	6.50	3.78
0.005	0.0271	1.23	2.67	1.89	5.15	0.288	6.41	4.07

Measured phase velocities and calculated elastic moduli for MLG:TiO$_2$-epoxy nanocomposites.

$\varphi_{f,m1}+\varphi_{f,m2}$, [1]	$\varphi_{f,v1}+\varphi_{f,v2}$, [1]	V_S, $\times 10^{-3}$ m·s^{-1}	V_L, $\times 10^{-3}$ m·s^{-1}	μ_C, $\times 10^{-9}$ N·m^{-2}	λ_C, $\times 10^{-9}$ N·m^{-2}	v_C, [1]	K_C, $\times 10^{-9}$ N·m^{-2}	E_C, $\times 10^{-9}$ N·m^{-2}
0.000	0.000	1.13	2.55	1.53	4.74	0.304	5.76	3.39
0.015	0.0055	1.15	2.61	1.63	5.15	0.306	6.24	3.63
0.020	0.0082	1.20	2.59	1.79	4.75	0.285	5.94	3.83
0.030	0.0136	1.16	2.66	1.68	5.49	0.310	6.61	3.77

[3, 7, 25, 40, 41], and theoretical methods [42–44].

It is generally accepted that polymer/solid interface are promoted by different forces such as covalent bonding, dipole-dipole attraction or van der Waals interaction, which act on quite a short range, a few nm for the Van der Waals forces and only a few Å for any type of chemical bonds [45, 46]. Atomistic models are intimately linked to these forces that are considered to be responsible for the formation of the interphase layers. Therefore, the values of the interphase thickness obtained by atomistic modelling don't exceed few nm.

According to the taxonomy presented in [43], the quantities estimated for interphase regions in the polymer nanocomposites can be classified into three groups. The first group includes the parameters converging on the scale of several monomer diameters, such as density, bond orientation, and monomer mobility. The second group contains the parameters which converge on the scale of the radius of gyration (R_g), such as deformation, orientation, and mobility of entire polymer chains. The third group encompasses quantities converging on scales larger than R_g, such as certain elastic constants, composition in cured networks and block copolymer structures. The space charge density, conductivity, permittivity and breakdown strength can also be included into the third group.

In particular, when employing the technique based on exploiting the structure or dynamics of entire polymer chains to estimate the interphase thickness, the value from about 2 to 3 R_g is usually obtained [42]. For the DGEBA-epoxy resins, the value $R_g \sim 12$ - 14 nm has been obtained [44].

Therefore, further comparison have been carried out for the fixed anatase-loading $\varphi_{f,m2}$ 0.01 (which corresponds to $\varphi_{f,v2} = 0.00288$), with varying MLG-content of $0 < \varphi_{f,v1} \leq 0.02$. The data are presented in Table 1b.

Comparison the data given in Tables 1a and 1b shows that depositing anatase on MLG-nanoplatelets enhances an impact of such a hybrid filler on the elastic moduli – they increase with increasing $\varphi_{f,v1}$ up to 16 % (as for λ at $\varphi_{f,m1}+ \varphi_{f,m2} = 0.30$) though in a monotonous manner.

The enhanced impact of MLG:TiO$_2$-hybrid nanoparticles on epoxy's molecular structure as compared to an impact of bare MLG-nanoplatelets can be explained by that the interface area enlarge further. Some possible physical mechanisms responsible for enhancement of interface interaction and thus for enlarging the interface area.

One mechanism may be related with a variation in electric charge density distribution along basal planes of the nanoparticles and within adjacent interphase regions due to relatively high dielectric permittivity of anatase particles. Indeed, it is known [47], that strong ionic polarization in titanium comes from the presence of Ti^{4+} and O^{2-} ions, and therefore it has a high dielectric permittivity for particles of both micrometer and nanometer sizes. Recent studies [48] confirmed this conclusion: here, for the 13-nm-sized TiO$_2$ particles it was found that the relative dielectric permittivity in the frequency range of 10^3 to $5 \cdot 10^6$ Hz makes about 60 and does not depend on frequency at temperatures from 30 to 90 °C. In accordance with the multilayered model proposed for the interphase regions in [49], when the difference between the dielectric permittivity of adjacent phases increases, the double electric layers emerge and the interphase region thickness increases.

Another plausible mechanism for enhancement of particle-chain interaction may be related to a circumstance that depositing anatase on MLG-nanoplatelets results in increasing their its mass (see calculation given in Table 2). It, in turn, causes lowering mobility for the hybrid particles during the curing process. Also, the difference in thermal conductivities between graphene and TiO$_2$ should be taken into account as a factor, which leads to increasing temperature gradients around the nanoparticles during the curing the nanocomposite. Gradients and, thus, increasing a strength of interaction among active surface sites and macromolecular chains. As a consequence, both the decreased mobility of MLG:TiO$_2$-hybrid nanoparticles and the temperature gradients promote a turbulence of mass microstreams, which play a key role in forming composite's molecular structure [50], namely in

Table 2

Numbers of the MLG (n_1) and TiO$_2$ (n_2) nanoparticles, the mass of the hybrid MLG:TiO$_2$-hybrid nanoparticle ($m_1 + \Delta m$), and the ratio ($m_1+\Delta m$)/m_1.

$M_1=\varphi_{f,m1} \times 1$ g, g	n_1, $\times 10^{-9}$	n_2 $\times 10^{-12}$	n_2/n_1	Δm, $\times 10^{12}$ g	$m_1+\Delta m$, $\times 10^{12}$ g	$1+ m_1/\Delta m$
0.005	1.764	4.547	2577	5.688	8.501	3.00
0.01	3.529	4.547	1289	2.834	5.668	2.00
0.02	7.058	4.547	644.3	1.417	4.251	1.50
0.05	17.64	4.547	257.7	0.567	3.401	1.20

increasing the cross linking degree (CLD) and density of entanglements of macromolecular chains around the particles. A network of entanglement nods means increasing interaction energy among macromolecular chains, i. e. increasing elastic constants, because the latter are the second derivatives of the nanocomposite's free energy over the elastic deformation [38].

Table 2 gives numerical estimations for the following quantities: 1) the numbers of both graphene nanoplatelets (n_1) and anatase nanoparticles (n_2), per unit mass (1 g) of the nanocomposites, 2) the ratio n_2/n_1, 3) mass increments ($\Delta m = m_2 \cdot n_2/n_1$) for the hybrid nanoparticle, and 4) the mass ratio ($m_1+\Delta m$)/m_1 in the assumption that anatase nanoparticles are distributed uniformly among the nanoplatelets.

In this calculation, the following values for particles volumes (V_1 and V_2) and masses (m_1 and m_2) have been used:

$V_1 = 5 \cdot 10^{-6}$ cm $\cdot$ $(5 \cdot 10^{-4}$ cm$)^2 \sim 1.25 \cdot 10^{-12}$ cm^3,

$V_2 = (4\pi/3) \cdot (5 \cdot 10^{-6}$ cm$)^3 \sim 5.23 \cdot 10^{-16}$ cm^3,

$m_1 = \rho_{f1} V_1 \sim 2.834 \cdot 10^{-12}$ g, $m_2 = \rho_{f2} V_2 \sim 2.199 \cdot 10^{-15}$ g.

One can see that the mass increment Δm, the mass ratio ($m_1+ \Delta m$)/m_1 are of substantial values.

However, it should be noted that both the mechanisms are also accompanied with breaking the chains. Indeed, the effect of decreasing CLD takes place in the composites [51, 52]. That effect plays for local decreasing the free energy in the interphase areas and thus for decreasing the overall elastic constant of the composites. Therefore, the dependence of the latter on the filler's concentration φ_f is of a nonmonotonous character (see Table 1).

Conclusions

The results obtained show that surface modification of multilayered graphene nanoplatelets with anatase nanoparticles allows to control surface reactivity of the formers and thus to impact the molecular structure of thermosets, in particular epoxy resins. However, quantitative estimation for an efficiency of such the impact requires further studies on concentration effects of the hybrid nanoparticles on electrical and thermal properties of the nanocomposites.

Nadtochiy A.B. – Ph.D. (Physical and Mathematical Sciences), Senior Researcher;

Gorelov B.M. – Doctor of Physical and Mathematical Sciences, Professor;

Polovina O.I. – Ph.D. (Physical and Mathematical Sciences), Researcher;

Shulga S.V. – Ph.D. (Chemistry), Researcher;

Korotchenkov O.O. – Doctor of Physical and Mathematical Sciences, Professor;

Gorb A.M. – Ph.D. (Physical and Mathematical Sciences), Researcher.

[1] J.A. King, D.R. Klimek, I. Miskioglu, G.M. Odegard, J. Compos. Mater. 49(6), 659 (2015); https://doi.org/10.1177/0021998314522674.

[2] A.S. Sarvestani, Int. J. Solids Struct. 40(26), 7553 (2003); https://doi.org/10.1016/S0020-7683(03)00299-3.

[3] R. Atif, I. Shyha, F. Inam, J. Compos. Mater. 51(2), 209 (2017); https://doi.org/10.1177/0021998316640060.

[4] R. Atif, I. Shyha, F. Inam, Polymers 8(8), 281 (2016); https://doi.org/10.3390/polym8080281.

[5] R Atif, F. Inam, Graphene 5(2), 96 (2016); https://doi.org/10.4236/graphene.2016.52011.

[6] D.G. Papageorgiou, I.A. Kinloch, R.J. Young, Prog. Mater. Sci. 90, 75 (2017); https://doi.org/10.1016/j.pmatsci.2017.07.004.

[7] Fu Shaoyun, Sun Zheng, Huang Pei, Li Yuanqing, Hu Ning, Nano Mater. Sci. 1(1), 2 (2019); https://doi.org/10.1016/j.nanoms.2019.02.006.

[8] M.A.G. Benega, W.M. Silva, M.C. Schnitzler, R.J.E. Andrade, H. Ribeiro, Polym. Test. 98, 107180 (2021); https://doi.org/10.1016/j.polymertesting.2021.107180.

[9] B.M. Gorelov, A.M. Gorb, O.I. Polovina, A.B. Nadtochiy, D.L. Starokadomskiy, S.V. Shulga, V.M. Ogenko, Nanosistemi, Nanomater. Nanotehnologii 14(4), 527 (2016).

[10] B. Gorelov, A. Gorb, A. Nadtochiy, D. Starokadomsky, V. Kuryliuk, N. Sigareva, S. Shulga, V. Ogenko, O. Korotchenkov, O. Polovina, J. Mater. Sci. 54(12), 9247 (2019); https://doi.org/10.1007/s10853-019-03523-7.

[11] Nadtochiy, B. Gorelov, O. Polovina, S. Shulga, O. Korotchenkov, J. Mater. Sci. 56(25), 14047 (2021); https://doi.org/10.1007/s10853-021-06134-3.

[12] C.D. Reddy, S. Rajendran, K.M. Liew, Nanotechnology 17(3), 864 (2006); https://doi.org/10.1088/0957-4484/17/3/042.

[13] M.D. Stoller, S.J. Park, Y.W. Zhu, J.H. An, R.S. Ruoff, Nano Lett. 8(10), 3498 (2008); https://doi.org/10.1021/nl802558y.

[14] C. Lee, X.D. Wei, J.W. Kysar, J. Hone, Science 321(5887), 385 (2008); https://doi.org/10.1126/science.1157996.

[15] M.J. Allen, V.C. Tung, R.B. Kaner, Chem. Rev. 110(1), 132 (2010); https://doi.org/10.1021/cr900070d.

[16] R. Verdejo, M.M. Bernal, L.J. Romasanta, M.A. Lopez-Manchado, J. Mater. Chem. 21(10), 3301 (2011); https://doi.org/10.1039/c0jm02708a.

[17] Y.J. Liu, Z.H. Tang, Y. Chen, S.W. Wu, B.C. Guo, Compos. Sci. Technol. 168, 214 (2018); https://doi.org/10.1016/j.compscitech.2018.10.005.

[18] H.L. Yang, F. Cai, Y.L. Luo, X. Ye, C. Zhang, S.Z. Wu, Compos. Sci. Technol. 188, 107971 (2020); https://doi.org/10.1016/j.compscitech.2019.107971.

[19] H.Y. Yan, Y.X. Tang, W. Long, Y.F. Li, J. Mater. Sci. 49(15), 5256 (2014); https://doi.org/10.1007/s10853-014-8198-z.

[20] W. Park, Y.F. Guo, X.Y. Li, J.N. Hu, L.W. Liu, X.L. Ruan, Y.P. Chen, J. Phys. Chem. C. 119(47), 26753 (2015); https://doi.org/10.1021/acs.jpcc.5b08816.

[21] X. Shen, Z.Y. Wang, Y. Wu, X. Liu, Y.B. He, J.K. Kim, Nano Lett. 16(6), 3585 (2016); https://doi.org/10.1021/acs.nanolett.6b00722.

[22] N. Burger, A. Laachachi, M. Ferriol, M. Lutz, V. Toniazzo, D. Ruch, Prog. Polym. Sci. 61, 1 (2016); https://doi.org/10.1016/j.progpolymsci.2016.05.001.

[23] M. Monti, M. Rallini, D. Puglia, L. Peponi, L. Torre, J.M. Kenny, Compos. A: Appl. Sci. Manuf. 46, 166 (2013); https://doi.org/10.1016/j.compositesa.2012.11.005.

[24] D. Ciprari, K. Jacob, R. Tannenbaum, Macromolecules 39(19), 6565 (2006); https://doi.org/10.1021/ma0602270.

[25] D. Pitsa, M.G. Danikas, Nano 6(6), 497 (2011); https://doi.org/10.1142/s1793292011002949.

[26] W.X. Peng, S. Rhim, Y. Zare, K.Y. Rhee, Polym. Compos. 40(3), 1117 (2019); https://doi.org/10.1002/pc.24813.

[27] M. Pakseresht, R. Ansari, M.K. Hassanzadeh-Aghdam, Proc. Inst. Mech. Eng. Pt. L J. Mater. Des. Appl. 234(7), 910 (2020); https://doi.org/10.1177/1464420720916857.

[28] H.M. Shodja, A.S. Sarvestani, J. Appl. Mech.-T. Asme. 68(1), 3 (2001); https://doi.org/10.1115/1.1346680.

[29] Z.Y. Xia, S. Pezzini, E. Treossi, G. Giambastiani, F.Corticelli, V.Morandi, A. Zanelli, V. Bellani, V. Palermo, Adv. Funct. Mater. 23(37), 4684 (2013); https://doi.org/10.1002/adfm.201203686.

[30] K. Eller, E. Henkes, R. Rossbacher, H. Höke, Amines, Aliphatic. Ullmann's Encyclopedia of Industrial Chemistry (Wiley-VCH Verlag GmbH & Co. KGaA, Weinheim, 2002).

[31] J. Kanzow, V. Zaporojtchenko, H. Nabika, M. Mizuhata, S. Deki, F. Faupel, Positron Annihilation, Icpa-13, Proceedings 445(6), 313 (2004); https://doi.org/10.4028/www.scientific.net/MSF.445-446.313.

[32] B. Lüthi, Physical Acoustics in the Solid State (Springer, Berlin, 2005).

[33] D. Royer, E. Dieulesaint, Elastic Waves in Solids I: Free and Guided Propagation. (Springer, Berlin, New York, 2000).

[34] K.X. Fu, Q. Xie, F.C. Lu, Q.J. Duan, X.J. Wang, Q.S. Zhu, Z.Y. Huang, Polymers 11(6), 975 (2019); https://doi.org/10.3390/polym11060975.

[35] https://www.americanelements.com/graphene-1034343-98-0.

[36] T.J. Ahrens, Mineral physics and crystallography: a handbook of physical constants. (American Geophysical Union, Washington, 1995).

[37] M.A. Isakovich, General Acoustics (Nauka, Moscow, 1973). [in Russian].

[38] L.D. Landau, L.P. Pitaevskii, A.M. Kosevich, E.M. Lifshitz, Theory of elasticity (Butterworth-Heinemann, 1986).

[39] Recent Advances in Structural Integrity Analysis: Proceedings of the International Congress (APCF/SIF-2014) (Elsevier Academic Press, Amsterdam, 2015).

[40] R. Rohini, P. Katti, S. Bose, Polymer 70(23), A17 (2015); https://doi.org/10.1016/j.polymer.2015.06.016.

[41] S. Zhao, H. Chang, S. Chen, J. Cui, Y. Yan, Eur. Polym. J. 84, 300 (2016); http://doi.org/10.1016/j.eurpolymj.2016.09.036.

[42] H. Eslami, M. Rahimi, F. Müller-Plathe, Macromolecules 46(21), 8680 (2013); https://doi.org/10.1021/ma401443v.

[43] E. Voyiatzis, M. Rahimi, F. Muller-Plathe, M.C. Böhm, Macromolecules 47(22), 7878 (2014); https://doi.org/10.1021/ma500556q.

[44] H. Park, I. Chung, M. Cho, J. Polym. Sci. 58, 1617(2020); https://doi.org/10.1002/pol.20200130.

[45] F.H. Gojny, M.H.G. Wichmann, B. Fiedler, I.A. Kinloch, W. Bauhofer, A.H. Windle, K. Schulte, Polymer 47(6), 2036 (2006); https://doi.org/10.1016/j.polymer.2006.01.029.

[46] C. Wehlack, W. Possart, J.K. Kruüger, U. Müller, Soft Mater. 5, 87 (2007); https://doi.org/10.1080/15394450701554536.

[47] L.D. Zhang, H.F. Zhang, G.Z. Wang, C.M. Mo, Y. Zhang, Phys. Status Solidi (A) 157(2), 483 (1996); https://doi.org/10.1002/pssa.2211570232.

[48] S. Sagadevan, Am. J. Nano Res. Appl. 1(1), 27 (2013); https://doi.org/10.11648/j.nano.20130101.16.

[49] T. Tanaka, M. Kozako, N. Fuse and Y. Ohki, IEEETrans. Dielectr. Electr. Insul. 12(4), 669 (2005); https://doi.org/10.1109/TDEI.2005.1511092.

[50] V.U. Novikov, G.V. Kozlov, Russian Chem. Reviews 69(4), 347 (2000); https://doi.org/10.1070/RC2000v069n04ABEH000523.

[51] H. Ribeiro, W.M. Silva, M.-T.F. Rodrigues, J.C. Neves, R. Paniago, C. Fantini, H.D.R. Calado, L.M. Seara, G.G. Silva, J. Mater. Sci. 48,7883 (2013); https://doi.org/10.1007/s10853-013-7478-3.

[52] K.W. Putz, M.J. Palmeri, R.B. Cohn, R.Andrews, L.C. Brinson, Macromolecules 41(18), 6752 (2008); https://doi.org/10.1021/ma800830p.

А.Б. Надточій[1], Б.М. Горєлов[2], О.І. Половина[1], С.В. Шульга[2],
О.О. Коротченков[1], А.М. Горб[1]

Швидкість звуку в епоксидних нанокомпозитах на основі графена

[1]Київський національний університет імені Тараса Шевченка, Київ, Україна, nadtku@univ.kiev.ua
[2]Інститут хімії поверхні ім. О.О. Чуйка Національної академії наук України, Київ, Україна, bgorel@ukr.net

Пружні властивості нанокомпозитів на основі епоксидної смоли (ЕНК), наповнених «чистими» багатошаровими графеновими нанопластинками (БШГ) та «гібридними» БШГ, на які осаджено наночастинки діоксиду титана, було тестовано за допомогою фазо-частотного ультразвукового зондування в режимі неперервного збудження (УЗЗ). Полімерною матрицею для цих нанокомпозитів слугувала діанова епоксидна смола CHS-EPOXY 520, що затверджувалася діетилтриаміновим затверджувачем (ДЕТА). Графенові наночастинки з питомою площею поверхні S_f ~790 м^2/г складалися з декількох десятків слабо зв'язаних моноатомних шарів і мали базові поверхні середнього розміру 5×5 мкм^2. Масове навантаження ($\varphi_{f,m}$) нанокомпозитів «чистими» БШГ варіювалося в межах від 0.1% до 5.0 %. Наночастинки TiO$_2$ у формі анатазу мали середній діаметр 50 нм та питому площу поверхні 1500 м^2/г і додавалися до БГШ-нанокомпозитів у кількості 1 % по масі.

Пружні модулі БГШ-ЕНК та БГШ: TiO$_2$-ЕНК (а саме, сталі Ламе, модуль Юнга, модуль всебічного стиснення та коефіцієнт Пуассона) показали незначні зміни зі зміною $\varphi_{f,m}$, незалежно від типу нанопластинок. Однак, вплив гібридних БГШ:TiO$_2$-нанопластинок на пружні модулі смоли виявився більш сильним, ніж вплив «чистих» БГШ. Цей результат показує можливість змінювати молекулярну структуру епоксидних смол шляхом впливу на реакційну здатність поверхні БГШ, які додаються у смолу.

Ключові слова: багатошарові графенові нанопластинки, наночастинки анатазу, епоксидні нанокомпозити, ультразвукове зондування, пружні модулі.